Current Biology 21, 1259–1267, August 9, 2011 ©2011 Elsevier Ltd All rights reserved DOI 10.1016/j.cub.2011.06.002

Article

Limiting Amounts of Centrosome Material Set Centrosome Size in *C. elegans* Embryos

Markus Decker,[1,4] Steffen Jaensch,[1,2,4] Andrei Pozniakovsky,[1] Andrea Zinke,[1] Kevin F. O'Connell,[3] Wolfgang Zachariae,[1] Eugene Myers,[2] and Anthony A. Hyman[1,*]

[1]Max Planck Institute for Cell Biology and Genetics, Dresden 01307 Germany

[2]Janelia Farm Research Campus, Howard Hughes Medical Institute, Ashburn, VA 20147, USA

[3]Laboratory of Biochemistry and Genetics, National Institute of Diabetes and Digestive and Kidney Diseases, National Institutes of Health, Bethesda, MD 20894, USA

Summary

Background: The ways in which cells set the size of intracellular structures is an important but largely unsolved problem [1]. Early embryonic divisions pose special problems in this regard. Many checkpoints common in somatic cells are missing from these divisions, which are characterized by rapid reductions in cell size and short cell cycles [2]. Embryonic cells must therefore possess simple and robust mechanisms that allow the size of many of their intracellular structures to rapidly scale with cell size.

Results: Here, we study the mechanism by which one structure, the centrosome, scales in size during the early embryonic divisions of *C. elegans*. We show that centrosome size is directly related to cell size and is independent of lineage. Two findings suggest that the total amount of maternally supplied centrosome proteins could limit centrosome size. First, the combined volume of all centrosomes formed at any one time in the developing embryo is constant. Second, the total volume of centrosomes in any one cell is independent of centrosome number. By increasing the amount of centrosome proteins in the cell, we provide evidence that one component that limits centrosome size is the conserved pericentriolar material protein SPD-2 [3], which we show binds to and targets polo-like kinase 1 [3, 4] to centrosomes.

Conclusions: We propose a limiting component hypothesis, in which the volume of the cell sets centrosome size by limiting the total amount of centrosome components. This idea could be a general mechanism for setting the size of intracellular organelles during development.

Introduction

The ways in which cells set the size of their intracellular structures is an important but unsolved problem [1]. Mechanisms must exist that allow the cell to scale the size of these structures as cells change size or fate during development and differentiation. For instance, in *C. elegans* embryos, the size of the mitotic spindle, centrosomes, and nucleus all change considerably with decreasing cell size. We have recently shown that the length of the mitotic spindle in *C. elegans* embryos is set in part by the size of the centrosomes [5]. Smaller cells have smaller centrosomes, resulting in smaller spindles. If the size of a centrosome is reduced in any particular cell, this results in a consequent reduction of spindle size. These experiments suggested that centrosome size responds in some way to the size of the cell.

The centrosome is the major microtubule-organizing center (MTOC) of a cell. In its center, each centrosome harbors a pair of barrel-shaped centrioles, which define the position of centrosome growth, whereas the number of centrioles present defines the number of centrosomes [6, 7] that can form per cell. Surrounding a centriole pair is an amorphous mass of protein commonly referred to as the pericentriolar material (PCM). Although no ultrastructural insights have been obtained to date, the PCM is believed to consist of an interconnected lattice-like structure [8] composed of coiled-coil proteins [9] that acts as a nucleation template for various effector molecules such as kinases and other centrosomal proteins that confer the functionality to the centrosome in terms of microtubule nucleation, anchoring, and dynamics [2].

The size of centrosomes is governed by a process termed maturation, in which centrioles gradually accumulate PCM [8]. The maturation process begins in interphase and continues throughout the cell cycle, culminating during mitosis, when centrosomes reach their full size. At the end of mitosis, centrosomes transition from maturation to disintegration through the loss of pericentriolar material, before beginning the growth cycle again [2]. It is thought that a cell sets the size of its centrosomes by controlling the maturation process, but little is known about how maturation is controlled outside of the fact that it requires the kinase Aurora A [10] and the coiled-coil proteins SPD-2 [3, 11] and SPD-5 [12].

Results

Final Centrosome Size Is Reached at Metaphase

To analyze the kinetics of centrosome growth through both the cell cycle and development, we collected Z stacks of between 30 and 50 slices over time and used a custom-written algorithm to analyze centrosome size in the stacks [13] (see Movie S1 and Movie S2 available online). This allowed us to analyze with unprecedented accuracy the growth of centrosomes in about 1000 embryos during the course of this project. Figure 1A shows a growth curve of centrosome maturation at the first cell division of a *C. elegans* embryo taking γ-tubulin::GFP [14–16] as a proxy for centrosome size. The centrosome initiates growth at around 650 s before nuclear envelope breakdown, grows continuously through the cell cycle as it matures, and eventually disintegrates with the onset of anaphase. The disintegration of a centrosome in *C. elegans* at anaphase is due in part to cortical pulling forces, which complicates the problem of quantifying centrosome size [17]. To circumvent this difficulty, we examined centrosome growth in cells with compromised cortical pulling forces by depleting GPR-1/2 [18] using RNA interference (RNAi). Using this approach, we showed that the kinetics of centrosome growth are roughly identical with and without force generation until ~150 s after nuclear envelope breakdown

[4]These authors contributed equally to this work

*Correspondence: hyman@mpi-cbg.de

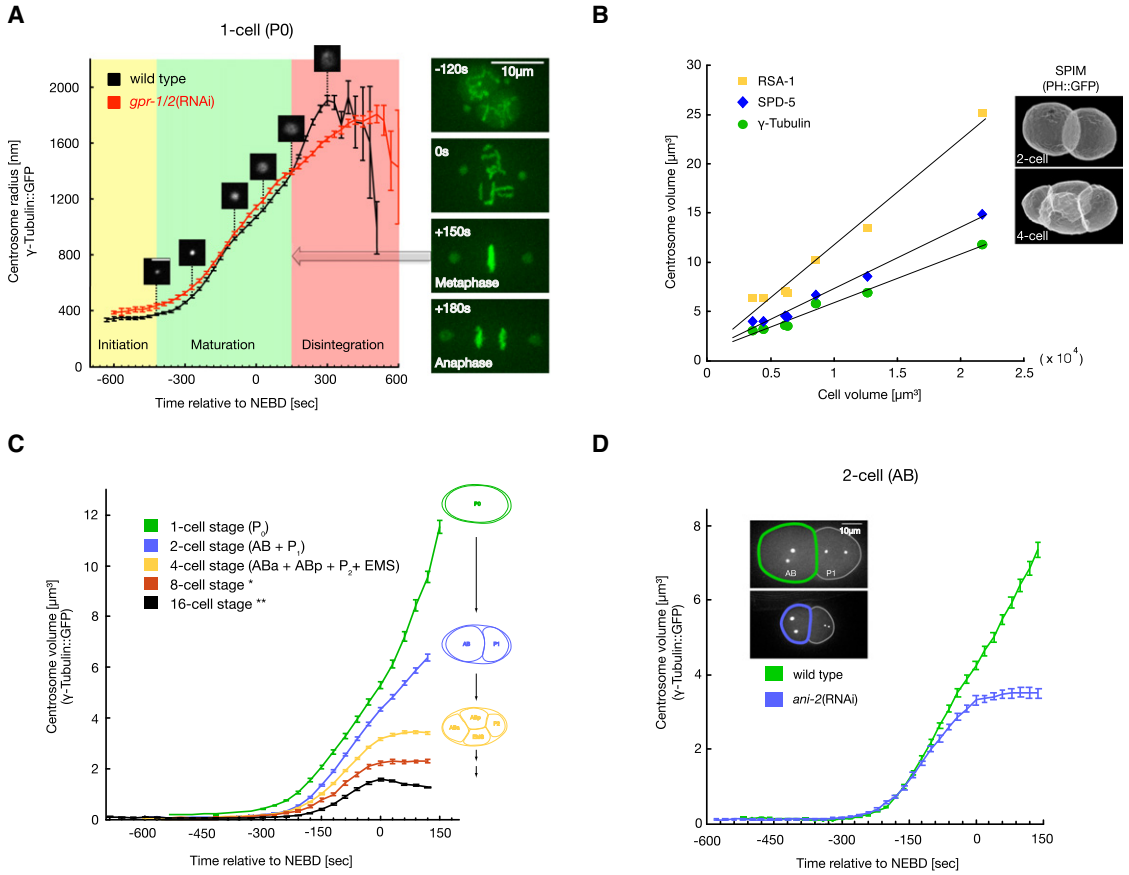

Figure 1. Centrosome Size Is Cell Fate Independent and Scales Proportionately with Cell Size

(A) Centrosome size in P_0. Left: graph showing the increase of centrosome radius with time from an average of 20 wild-type and 7 *gpr-1/2*(RNAi) embryos. Error bars are standard error of the mean. Scale bar in centrosome clippings is 3 μm. Right: image sequence taken of embryos expressing both γ-tubulin::GFP and histone::GFP, illustrating that metaphase correlates with the transition from maturation to disintegration. All images are maximum projections of confocal Z stacks.

(B) Centrosome size scales linearly with cell size. The graph shows centrosome volume plotted against respective cell volume for three different centrosomal markers. Linear fits are least square fits. Final centrosome size was measured at metaphase time depending on cell type (e.g., 150 s after nuclear envelope breakdown [NEBD] for P_0). Volume measurements for individual cell types were obtained from digital 3D reconstructions of embryos expressing a fusion between GFP and a PH domain (n = 5). The inset images show reconstructions of an embryo in the 2- and 4-cell stages.

(C) Centrosome size through development. The graph shows how centrosomal growth rate and centrosome volume decrease over time from the 1- to the 16-cell stage. The data comprise an averaged set of 1- to 4-cell-stage embryos (n = 25) and 8- to 16-cell-stage embryos (n = 6) all expressing γ-tubulin::GFP. Error bars are standard error of the mean. Because of signal attenuation along the z axis, not all 16 centrosomes of an embryo in the 8-cell stage contribute to the graph (*). Similarly, not all 32 centrosomes of an embryo in the 16-cell stage contribute to the graph, and only AB lineage centrosomes were analyzed (**).

(D) Centrosome size in smaller AB cells. The graph shows growth rates in AB cells of *ani-2*(RNAi) embryos. Assuming ellipsoidal shape, embryo volume was estimated by measuring the embryo area in maximum-intensity z projections and the embryo thickness in maximum-intensity y projections. Snapshot images are all maximum projections of confocal Z stacks. Scale bar represents 10 μm.

in cells of the one-cell stage (P_0) (Figure 1A). Beyond this point, the two curves distinctly diverged from one another. We obtained analogous results for both cells of the two-cell stage (AB, P_1) and all cells of the four-cell stage (ABp, ABa, P_2, EMS) (see Figure S1 for ABp). This suggested to us that any growth occurring after this point of divergence is a consequence of pulling forces and not active recruitment. Because these time points correspond to the time of metaphase-anaphase transition in the respective cell type, we defined final centrosome size as the size at metaphase.

Centrosomes Can Quantitatively "Read" Cell Size and Adjust Their Size Relative to Cell Size by Changing Their Growth Kinetics

We next measured cell size during early development using single plane illumination microscopy (SPIM)-derived 3D time-lapse measurements and correlated centrosome size with cell size at metaphase. To this end, we labeled cell membranes with a PH domain fused to GFP and used γ-tubulin::GFP, RSA-1::GFP [19], and SPD-5::GFP as proxies for centrosome size. We were intrigued to find that for all three centrosomal markers tested, centrosome size not only correlates with cell size, as previously shown [5] but in fact scales proportionately with cell size (Figure 1B). This result suggested to us that centrosomes are in some way able to quantitatively "read" cell size and adjust their size accordingly.

To examine in detail how centrosome size changes as cells get smaller, we derived kinetic profiles for centrosome growth up to the 16-cell stage (Figure 1C) using γ-tubulin::GFP as a marker for centrosome size. Two distinct features of the resulting growth curves are suggestive. First, starting from the two-cell stage, the centrosomes grow more slowly when cells

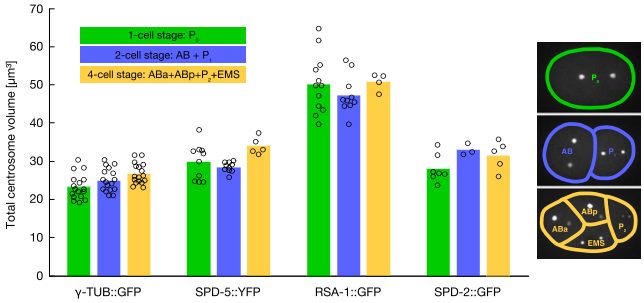

Figure 2. Total Centrosome Volume Is Conserved through Development

Comparison of the total sum of centrosome volumes between the 1-, 2- and 4-cell stages. Centrosome volume was determined in each individual cell at metaphase. γ-tubulin: n = 17/17/17; SPD-5: n = 9/10/5; RSA-1: n = 12/10/4; SPD-2 (TH42): n = 7/3/5 for 1-/2-/4-cell stages. Snapshot images are all maximum projections of confocal Z stacks.

are smaller. Second, starting at the four-cell stage, centrosome size plateaus before nuclear envelope breakdown (Figure 1C). We did not see a plateau at the one- and two-cell stages but suspect that this is because any plateau would occur close to the metaphase-anaphase transition in these cells and therefore be obscured by GPR-1/2-dependent and -independent pulling forces [20]. We obtained similar results for RSA-1::GFP and SPD-5::GFP (data not shown). Taken together, these data clearly show that the decline in the size of centrosomes during development is due to a change in their growth kinetics.

Centrosome Size Is Cell Fate Independent and Directly Set by Cell Size

One possibility is that cells regulate their centrosome growth rate in a cell-fate-specific manner. Another possibility is that the mechanisms controlling growth rate remain constant through development but that these mechanisms are innately affected by cell size. To distinguish these ideas, we varied the size of embryos using *ani-2* RNAi [21]. *ani-2* encodes a *C. elegans* anillin, which is required for precise determination of oocyte size. Smaller embryos make smaller cells, allowing us to compare the size of centrosomes in a varied range of cell sizes for any particular cell type. In AB cells of embryos that are 42% ± 5% (standard deviation [SD]) of wild-type size as shown in Figure 1D, centrosomes initially grow slower than centrosomes in wild-type cells. After this initial growth, the size then reaches a plateau, which is never seen in centrosomes of AB cells of wild-type size. Other cells (P_0, P_1, ABa, ABp, EMS, and P_2) showed a similar variation in growth rates upon depletion of ANI-2 (data not shown). Interestingly, we found that the changes in centrosomal growth rate during development are similar to those caused by making cells smaller by means of *ani-2*(RNAi). We quantified this by computing a derivative of the average growth curves of centrosomes (see Experimental Procedures) through development and after anillin RNAi. This approach yielded a maximum growth rate of centrosomes in a two-cell wild-type embryo of 0.022 $\mu m^3/s$, whereas centrosomes in four-cell embryos grow at 0.017 $\mu m^3/s$. Centrosomes in two-cell *ani-2*(RNAi) embryos that are 42% ± 5% (SD) of wild-type size grow at 0.018 $\mu m^3/s$. These experiments show that centrosome size is directly set by cell size during development and is independent of lineage. They further show that the plateau in growth that occurs in later divisions is a consequence of cell size and not of a developmental shift.

Total Centrosome Volume Is Conserved through Development and Independent of Centrosome Number

How can cell size set the size of a centrosome? The fact that growth of centrosomes tends to plateau and that centrosome size scales proportionately with cell size suggests that centrosome size is limited by the cytoplasmic amounts of one or more limiting components. This idea predicts that the total volume of all centrosomes during development should stay constant as the maternal cytoplasm of the first cell is partitioned into many cells during development. To test this idea, we quantified total centrosome volume during development (Figure 2). These measurements show clearly that for the four centrosomal components we measured, total centrosome volume stays constant in the embryo up to the four-cell stage. Beyond the four-cell stage, the attenuation of the fluorescent signal along the Z direction does not allow reliable measurement of all centrosomes. We next tested whether centrosome volume was constant in any one particular cell by manipulating the number of centrosomes in the cell using two mutant alleles of the kinase ZYG-1. ZYG-1 is related to the kinase PLK-4/SAK and determines the number of centrioles in cells, and thereby the number of centrosomes [22]. Using these mutant kinase alleles, we were either able to decrease (Figure 3D) or increase (Figure 3E) centrosome number per cell. In all of these cases, the total centrosome volume per embryo roughly added up to a fixed amount, independent of the number of centrosomes (Figures 3A and 3C). Again we were intrigued to find that centrosome growth, unlike in wild-type, plateaus in the two-cell stage as the number of centrosomes increases (Figure 3B). We presume that this is due to the increased competition for limiting amounts of centrosomal material in the presence of many centrosomes. Finally, we also examined cells in which we varied the relative size of the two centrosomes by manipulating the amount of the centriole protein SAS-4 [23] and found that the total sum of centrosome volumes in these cells was again approximately constant (Figure S2). Taken together, the results from following total centrosome volume through development, and the results from manipulating centrosome number, show clearly that the total amount of centrosome material remains constant in the embryo. This provides compelling evidence that centrosome size could indeed be limited by the amount of components provided to the embryo by the maternal cytoplasm.

SPD-2 Amounts Limit Centrosome Size by Determining the Growth Rate of Centrosomes

Which proteins could set centrosome size? Work over the last decade has defined a number of centrosome components in *C. elegans*, together with a rough assembly pathway [2, 24]. These experiments have shown that three proteins, SPD-2 [3], SPD-5 [11], and AIR-1 [10], are required for the assembly of all other centrosome proteins. SPD-2 and SPD-5 are both coiled-coil proteins, of which only SPD-2 is conserved in other species [25], and AIR-1 encodes the *C. elegans* Aurora A kinase [26]. Depletion of these three proteins has previously been shown to affect centrosome size. We found that the reason for this is that RNAi directed against any of these components decreases the rate of centrosome growth (Figure S3).

To see whether the availability of SDP-2, SPD-5, or AIR-1 actually limits centrosome size, we sought to increase protein levels by introducing a single, additional copy of their respective genes into the genome. Introduction of an RNAi-resistant AIR-1 or SPD-5 transgene followed by the depletion of the

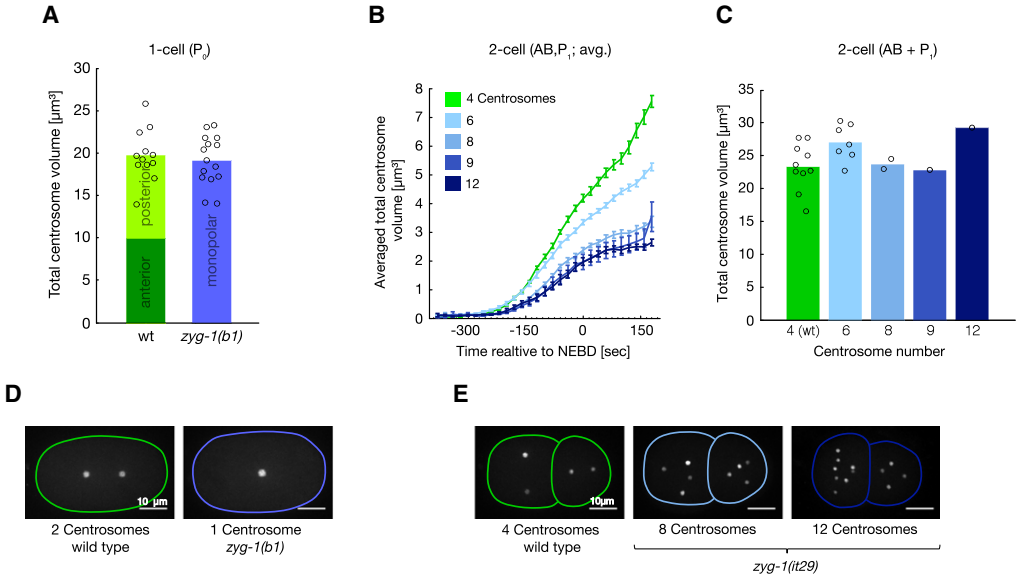

Figure 3. Total Centrosome Volume Is Independent of the Number of Centrosomes

(A) Bar chart showing total centrosome volume at metaphase in 1-cell-stage wild-type versus *zyg1(b1)* embryos. Wild-type: n = 12 embryos; *zyg1(b1)*: n = 15 embryos. Final centrosome size was measured at 150 s after NEBD (metaphase).

(B) Graph showing centrosome growth curves for 2-cell stage wild-type versus *zyg-1(it29)* embryos. Each curve is an average across all centrosomes in AB and P_1. Error bars are standard error of the mean. Wild-type: n = 10 embryos; *zyg-1(it29)*: n = 7/2/1/1 for 6/8/9/12 centrosomes per 2-cell-stage embryo.

(C) Bar chart showing total centrosome volume at metaphase of the same embryos used in (B).

(D) Representative images of 1-cell-stage *zyg-1(b1)* and respective wild-type embryos (both expressing γ-tubulin::GFP). Scale bars represent 10 µm. All images are maximum projections of confocal Z stacks.

(E) Representative images of 2-cell-stage *zyg-1(it29)* and respective wild-type embryos (both expressing γ-tubulin::GFP). Scale bars represent 10 µm. All images are maximum projections of confocal Z stacks.

respective endogenous protein did not have any effect on centrosome size (Figure S4). This result demonstrates that both transgenes are functional in vivo. Furthermore, because increasing the amount of protein does not change centrosome size, it further suggests that neither AIR-1 nor SPD-5 amounts act limiting on centrosome size. Interestingly, unlike AIR-1 and SPD-5, we found that SPD-2 protein levels are normally maintained within narrow limits, even in the presence of an additional SPD-2::GFP transgene (Figure S5). However, this regulation can be overcome by optimizing transgene codon usage [27], allowing us to raise SPD-2 protein expression beyond wild-type levels (Figure 4A). Increasing SPD-2 protein levels did increase centrosome size (Figures 4B and 4C, left panels), demonstrating that the size of the centrosome is related to the amount of SPD-2 protein in the cell. To investigate why centrosomes are bigger in cells with increased amounts of SPD-2, we derived growth kinetics of centrosomes in respective cells. These measurements clearly show that elevated amounts of SPD-2 protein increase the rate with which centrosomes grow (Figures 4B and 4C, right panels). Importantly, they also show that centrosomal growth eventually plateaus at a higher level compared to controls (Figure 4C, right panel), as would be expected when increasing the amount of a limiting component.

SPD-2 May Limit Centrosome Size by Acting as a PLK-1 Localizer

How can SPD-2 act limiting on centrosome size? We have recently shown by a modified two-hybrid analysis [28] that SPD-2 interacts with PLK-1, which is the gene that encodes polo-like kinase 1 in *C. elegans* [29, 30]. Polo kinase has been implicated in centrosome function in many different systems [4]. Yet, its role in *C. elegans* in this regard remains largely elusive. To investigate whether PLK-1 has a role in centrosome maturation, we partially RNAi-depleted PLK-1 in embryos expressing γ-tubulin::GFP. This resulted in a reduced centrosomal growth rate and consequently smaller centrosomes (Figure 5A).

We next tested the idea that the limiting effect of SPD-2 on centrosome size may be mediated by its ability to function as a PLK-1 localizer. To characterize the SPD-2/PLK-1 interaction in more detail, we performed glutathione S-transferase (GST)-pull-down experiments using baculovirus-expressed proteins. Using this approach, we were able not only to verify the previously reported interaction but also to detect a distinct mobility shift for the SPD-2 minimal interaction domain (MID) (Figure 5B). The observed shift was found to depend on the coexpression of the full-length kinase and could be reversed by phosphatase treatment, indicating that the SPD-2 MID is subject to PLK-1-mediated phosphorylation (Figure 5B). Phosphatase treatment furthermore demonstrated that the interaction is itself sensitive to the phosphorylation state of the proteins (Figure 5B). This finding stands in good agreement with the current concept that target binding of PLK-1 requires a priming kinase. In the context of our in vitro pull-down experiments, such priming function is presumably provided by the expression system used in our assay.

Next, we aimed to test whether the interaction between SPD-2 and PLK-1 is important for centrosome growth in embryos by specifically abolishing binding of PLK-1 to SPD-2. Point mutagenesis in combination with GST-pull-downs of baculovirus-expressed proteins indicated that a consensus site [31] in the SPD-2 MID comprising serine 232 and threonine 233 mediates binding to PLK-1 (Figures 6A and 6B). To

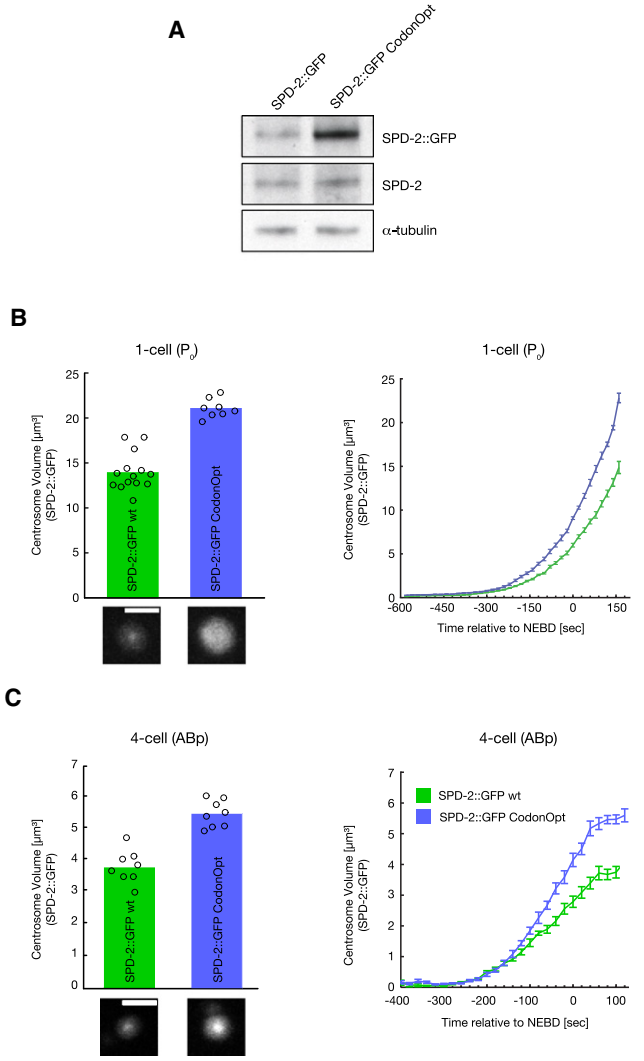

Figure 4. The Size of Centrosomes Is Sensitive to Total SPD-2 Amounts

(A) Western blot illustrating that codon optimization of SPD-2 (TH303) results in higher amounts of SPD-2::GFP compared to nonoptimized SPD-2 (TH257). α-tubulin was used as a loading control.

(B) Left: bar chart comparing centrosome volume in P_0 at metaphase in SPD-2::GFP embryos expressing different levels of SPD-2. Green bar: embryos expressing endogenous SPD-2 and SPD-2::GFP with native codon sequence; n = 7 embryos. Blue bar: embryos expressing endogenous SPD-2 and SPD-2::GFP with codon-optimized sequence; n = 4 embryos. The representative images show centrosomes at metaphase in one-cell embryos expressing different levels of SPD-2::GFP. Scale bar represents 3 μm. All images are maximum projections of confocal Z stacks. Right: centrosomal growth kinetics in P_0 for the same set of embryos. Error bars are standard error of the mean.

(C) Left: bar chart comparing centrosome volume in ABp at metaphase in SPD-2::GFP embryos expressing different levels of SPD-2. Green bar: embryos expressing endogenous SPD-2 and SPD-2::GFP with native codon sequence; n = 4 embryos. Blue bar: embryos expressing endogenous SPD-2 and SPD-2::GFP with codon optimized sequence; n = 4 embryos. The representative images show centrosomes at metaphase in four-cell embryos expressing different levels of SPD-2::GFP. Scale bar represents 3 μm. All images are maximum projections of confocal Z stacks. Right: centrosomal growth kinetics in ABp for the same set of embryos as in (B), illustrating that increasing levels of SPD-2 increase centrosome size by affecting growth rate. Error bars are standard error of the mean.

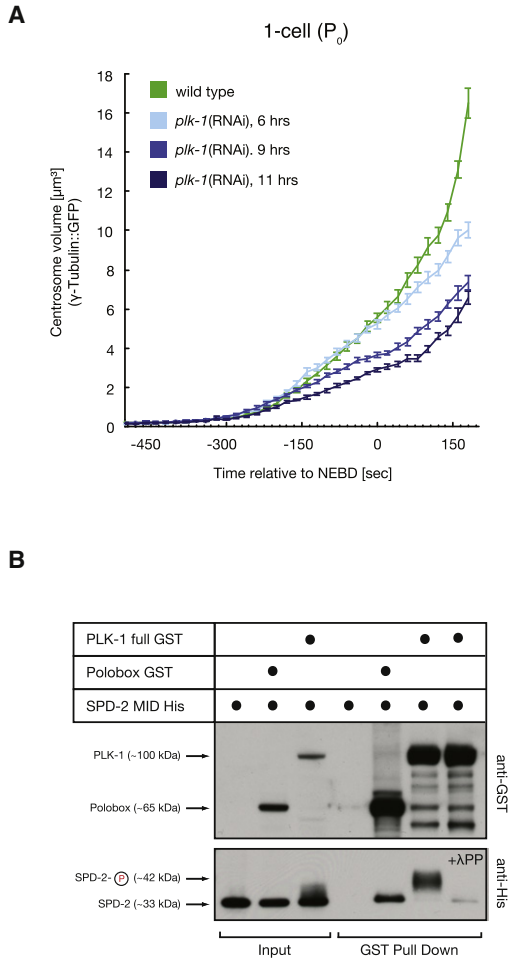

Figure 5. PLK-1 Affects Centrosome Maturation and Phosphorylates SPD-2

(A) Graph showing centrosome growth in 1-cell-stage embryos expressing γ-tubulin::GFP and subjected to various degrees of partial RNAi against *plk-1*; n = 12/8/7/6 (order of the given numbers corresponds to the order in the legend of the respective graph). Error bars are standard error of the mean.

(B) GST-pull-down assay demonstrating that the SPD-2 minimal interaction domain (MID) interacts with either full-length PLK-1 or its polobox. Furthermore, the observed phosphoshift of the SPD-2 MID and its interaction with PLK-1 is sensitive to treatment with lambda protein phosphatase (λPP). Pull-downs were performed on cleared lysates obtained from baculovirus-infected cells coexpressing either full-length GST-tagged PLK-1 or GST-tagged polobox and the HIS-tagged SPD-2 MID. The indicated molecular weights are based on migration behavior relative to a molecular weight standard.

eventually investigate the functional significance of the PLK-1/SPD-2 interaction in vivo, we generated a GFP-tagged SPD-2 transgene that was RNAi resistant at the nucleotide level and contained the two point mutations S232T and T233A. When we ran down the endogenous protein, the mutant transgene was able to support little centrosome growth (Figure 6C). Interestingly, even in the presence of the endogenous SPD-2 gene, embryos expressing the mutant transgene were severely compromised for centrosome growth (Figure 6C). This dominant effect of the SPD-2 point mutant presumably results from compensation (Figure S5) during which the endogenous wild-type copy becomes downregulated to accommodate the expression of the mutant transgene. Indeed, we found

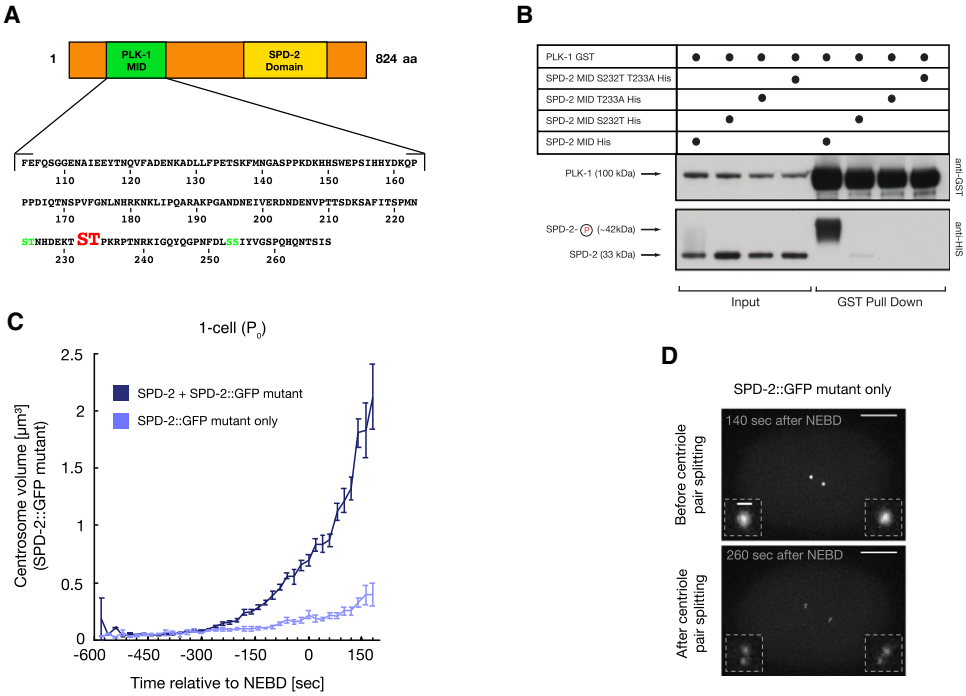

Figure 6. Abolishing the Binding between SPD-2 and PLK-1 Affects Centrosome Size

(A) Schematic representation of SPD-2 in *C. elegans*, with the conserved N-terminal SPD-2 domain depicted in yellow and the refined MID for PLK-1 in green. The MID contains three potential PLK-1 consensus binding motifs. Residues that were found to be crucial for PLK-1 binding are colored in red, whereas those that exhibited no effect are shown in green.

(B) GST pull-down assay demonstrating that point mutations S232T and T233A abolish binding and phosphorylation of the MID by PLK-1. Pull-downs were performed on cleared lysates obtained from baculovirus cells coexpressing full-length GST-tagged PLK-1 and one of four different HIS-tagged SPD-2 MIDs. The indicated molecular weights are based on migration behavior relative to a molecular weight standard.

(C) Growth curves of centrosomes in embryos expressing full-length SPD-2::GFP in which point mutations S232T and T233A were introduced (TH285). The construct was codon rendered in a specific region in order to make it RNAi resistant, enabling us to specifically deplete only endogenous SPD-2 in these embryos (see Experimental Procedures for details).

(D) Two snapshots of a 1-cell-stage embryo expressing mutant SPD-2::GFP before (140 s before NEBD) and after centriole pair splitting (260 s after NEBD). Endogenous SPD-2 was completely depleted (RNAi for 30 hr) prior to imaging. The small insets represent zoomed-in clippings of the embryo's centrosomes. Scale bars in insets represent 1 μm. All images are maximum projections of confocal Z stacks.

that RNAi directed against the mutant transgene could restore wild-type cell divisions (Figure S6A).

To check whether the observed defect in centrosome maturation in the S232T/T233A mutant is in fact due to the deficiency of mutant SPD-2 to localize PLK-1 to the centrosome, we quantified centrosomal PLK-1 levels in embryos expressing mutant SPD-2. The corresponding analysis clearly showed that the total centrosomal amounts of both PLK-1 and SPD-2 were severely reduced (Figures S6B–S6D). This correlation further solidifies the proposed SPD-2/PLK-1 relationship. Moreover, other pericentriolar proteins, such as γ-tubulin and SPD-5, were also found to be diminished (data not shown), reinforcing that centrosomal PLK-1 amounts are indeed a decisive factor in controlling the incorporation of key PCM components and thus centrosome size in general. Strikingly, however, centriole duplication, which also depends on SPD-2, was not affected when centrosome growth solely depended on the mutant SPD-2 transgene (Figure 6D). This fact suggests to us that SPD-2 has a PLK-1-dependent centrosome maturation function and a PLK-1-independent function in centriole duplication. Thus, we ultimately conclude that SPD-2 amounts could regulate centrosome size at least in part by limiting the amount of PLK-1 targeted to centrosomes.

Discussion

How could the amounts of a centrosome protein limit the size of centrosomes? It seems likely that the concentration of one or more centrosome components controls the reaction rate of the assembly process. Our experiments demonstrate that the concentration of one such rate-limiting protein, SPD-2, can indeed determine centrosome size. We propose that a limiting component will be allocated proportionately as cytokinesis divides the maternal cytoplasm into ever-smaller daughter cells. As a result of this process, each cell will only differ in terms of the total amount of limiting material it contains, but not in terms of its concentration. As centrosomes begin to grow in their respective cytoplasm, the cytoplasmic concentration of a limiting factor will gradually decrease as centrosomes bind and sequester material from the cytoplasm. Eventually, the cytoplasmic concentration will drop below a certain threshold that is not sufficient to support further growth. Inherent to this depletion system, centrosomal growth will cause the concentration of a size-limiting factor to drop faster with decreasing cell size. The threshold concentration should therefore be reached earlier in smaller cells, ultimately resulting in cell-size-dependent centrosome scaling. This prediction is supported by measurements of centrosomal

growth rates through development, which clearly show that plateau formation indeed occurs increasingly earlier as cells become smaller: ~60 s after nuclear envelope breakdown (NEBD) in the 4-cell stage, ~30 s after NEBD in the 8-cell stage, and approximately at NEBD in the 16-cell stage. Our proposed model implies that the centrosomal growth rate is dependent on the concentration of the limiting component. Hence, the changes in cytoplasmic concentration of limiting factors that take place when centrosomes mature are ultimately responsible for the fact that centrosomal growth eventually levels off. In support of this idea, increasing amounts of SPD-2::GFP increase the growth rate of centrosomes (Figures 4B and 4C) and, as would be suspected for this scenario, make them plateau on a higher level. Further evidence in this regard comes from the fact that growth rates slow down when centrosome number is increased in the cytoplasm (Figure 3B) and when cell size is reduced by anillin-2 RNAi (Figure 1D). Testing our idea in more detail will, among other things, require modeling as well as measuring protein concentration throughout the cell cycle. Measuring protein concentration has so far proved challenging as a result of the low cytoplasmic fluorescence and its inhomogeneity relative to the autofluorescent background signal of the embryo.

Our findings with regard to the central role of SPD-2 in centrosome size control stand in good agreement with recently published work in *Drosophila*. Specifically, centrosome size in *Drosophila* embryos was found to be controlled by the rate of Cnn incorporation at the centriole [32]. Importantly, Cnn incorporation is driven in part by its interaction with the centriolar protein DSpd-2, the fly homolog of *C. elegans* SPD-2. This result supports the notion that our proposed SPD-2-centered mechanism for centrosome size control is conserved throughout evolution.

Our data suggest that SPD-2 may act limiting in setting centrosome size by limiting the amount of PLK-1 that is targeted to centrosomes. In principle, this idea implies that PLK-1 amounts are not limiting and should therefore exceed those of SPD-2 in the embryo. Lowering PLK-1 amounts below those of SPD-2 should therefore lead to a reduction in centrosome size. Indeed, we found that partial RNAi depletion of PLK-1 reduces centrosome size. Further experiments examining the relative concentrations of these two proteins under RNAi conditions would be needed to reinforce this conclusion. According to the current working model, the polo-box-binding domain (PBD) of polo kinase binds to a phosphoepitope generated by a priming kinase [31, 33]. Although no direct experimental evidence is available as to what kinase might prime SPD-2 for PLK-1 binding in vivo, it is interesting to note that the polobox consensus binding site on SPD-2 is superimposed with a CDK-1/2 phosphorylation consensus site [34]. This hints at the possibility that a cyclin-dependent kinase (CDK) may act as the priming kinase, which would ensure that centrosome maturation is properly coupled to the progression of the cell cycle. Indeed, previous work has shown that *cdk-2*(RNAi) delays centrosome growth [35].

It is reasonable to assume that SPD-2 is an actual target of PLK-1 phosphorylation in vivo, although it is also conceivable that SPD-2 may simply localize the kinase in close proximity to its actual targets at the centrosome [36]. The actual mechanistic role of PLK-1-mediated phosphorylation for centrosome maturation remains elusive. Interestingly, the recent mapping of interaction domains for a set of key pericentriolar proteins [28] suggests that SPD-2 together with several other components may form a multiprotein complex in which SPD-5 appears to function as the central scaffold. Whether PLK-1-mediated phosphorylation has any role in the assembly of this potential complex or may even induce polymerization of this SPD-5 centered complex into a higher-order PCM structure will be an interesting direction for the future.

Controlling the size of a centrosome by limiting the amounts of one of its components requires tight control of the concentration of the protein that is limiting. This is true for all types of biological processes that are thought to be under control of substrate depletion, such as Turing-like substrate depletion models for cell polarity [37–39]. Control of protein amounts could come simply from the rate of synthesis and degradation inside the embryo, or from more complex mechanisms involving feedback. In principle, feedback mechanisms could respond to reduction of amounts of components in the cytoplasm as they are recruited onto centrosomes; in practice, however, the timescales of the 10 min cell cycles are probably too fast for the appropriate translational responses, although we know little about these rates. In fact, inhibition of transcription does not affect centrosome size (data not shown). These ideas suggest that a more concerted study of the turnover rates of individual proteins during development would be worthwhile.

There are data from a number of systems in which the size of intracellular contents scales with cell size. One classic example is the nucleus-to-cytoplasmic ratio [40]. Other examples are mitochondrial volume scaling with cell volume [41], mitotic spindle length scaling with cell size [5, 42], and rate of ring constriction during cytokinesis scaling with initial cell perimeter [43]. Although the idea of limiting components has been proposed for size control in some systems [44, 45], there is little experimental evidence to support it. However, a limiting component system, as we describe here, could be a general way of limiting the size of intracellular organelles in systems with fast cell cycles and rapidly changing cell volume. Its great advantage is to provide a robust and rapid system that takes advantage of the contribution of a defined amount of maternal cytoplasm to the embryo. In combination with a defined seed, such as a centriole, a limiting component would ensure that the size of the intracellular structure scales according to cell size. By examining the response of intracellular structures to increase and loss of the components of which they consist, it may be possible to identify components that limit the growth of other cellular structures.

Our experiments have focused on an early embryonic system, whose development depends on maternal cytoplasm. These cells have to quickly change the size of their components as cells rapidly divide through the early cell cycles; the mechanisms as we have described may be appropriate for such large and rapid changes in size. Whether similar mechanisms also apply in somatic systems, with longer cell cycles and smaller changes in cell size, is an important direction for future investigation.

Experimental Procedures

Worm Strains and RNA Interference

Maintenance of *C. elegans* worm strains was carried out according to standard protocols [1]. The following worm strains were used: DH1 (*zyg-1(b1)*), *zyg-1 (it29)* ([46]; gift from K.F.O.), OD58 (PH-domain::GFP) [2], TH27 (γ-tubulin::GFP), TH42 (SPD-2::GFP; CAI0.27), TH55 (RSA-1::GFP), TH231 (SPD-2::GFP; CAI0.27/fosmid), TH257 (SPD-2::GFP; CAI0.27), TH285 (SPD-2::GFP; S232T T233A), TH303 (SPD-2::GFP; CAI 0.37), TH327 (SPD-5::GFP; CAI 0.65), TH329 (AIR-GFP ; CAI 1.0). The five SPD-2 lines used in this study (TH42, TH231, TH257, TH285, and TH303) differ in their codon adaptation

index (CAI) [3]. The N terminus of the *spd-2* transgene in TH303 was codon optimized (Geneart) with respect to the codon bias in *C. elegans*, so that the overall CAI score increased from the native value of 0.27 (TH42, TH231, TH257, and TH285) to 0.37. In addition, in TH257, TH285, and TH303, the transgenic *spd-2* sequences feature a 551 bp C-terminal stretch that was also subjected to codon optimization. However, for this fragment, codons were chosen in a way that would not increase the CAI score but simply achieve maximal divergence to the native codons. In this way, respective lines were made resistant to the *spd-2* RNAi feeding clone that was used in this study (see below). Point mutations carried by the *spd-2* transgene in TH285 were introduced using the QuikChange Site-Directed Mutagenesis Kit (Stratagene). The AIR-1::GFP (TH329) and SPD-5::GFP (TH327) lines used in this study were also subjected to codon optimization (Geneart). Codon optimization was performed in a way that optimized condons scatter homogenously across the entire sequence length. The CAI score for *spd-5* was increased to 0.65 (TH327), and that of *air-1* was rendered to yield 1.0. As a result of this process, both TH327 and TH329 are RNAi-resistant compared to their endogenous counterparts when using the appropriate feeding clone listed below. All genes with the exception of TH231 (SPD-2::GFP; CAI0.27/fosmid) were cloned into a tagging plasmid (pAZ132), and expression was driven by the *pie-1* promotor. TH231 was generated by recombineering in a fosmid containing *spd-2* under its endogenous promotor, tagged with GFP at the C terminus [4]. All transgenic lines were created by microparticle bombardment as described [5]. Worms were subjected to both RNAi by injection and RNAi by feeding as previously described [6, 7]. The RNAi method used for each gene, as well as the region targeted, is indicated in the following list:

RNAi by Injection

Primer sequences for the regions targeted are as follows, with T3/T7 extensions underlined: *ani-2*: TAATACGACTCACTATAGGGAGACCACCAACGA CTCCAAACGTCAGATA, AATTAACCCTCACTAAAGGGTCTCGTCCG TTTC TTGTTTCT. Template: N2 genomic DNA.

RNAi by Feeding

The regions targeted by the feeding clone are flanked by the following primers: *sas-4*: AAACTGGTGGCACTGGATTC (forward primer), ATGAAC GATTTAGGCGTTGG (reverse primer); *gfp*: ATGAGTAAAGGAGAAGAACT (forward primer), TTTGTATAGTTCATCCATGC (reverse primer); *spd-2*: GAATGCATCAATGGCAGATG (forward primer), AATTTTGTGCCGGTACT TCG (reverse primer); *gpr-1/2*: GAGCCTTGTCGTAATAGGCG (forward primer), GATCCGCGTGAAATTTTTGT (reverse primer); *air-1*: ACGTGTCAG CAACGACACTC (forward primer), GTCCCGAGGAGAAAAGGAAC (reverse primer); *spd-5*: AACCATTACTGATATGGGGA (forward primer), CAAATGAA CAATTCTTTCAAGCA (reverse primer); *plk-1*: TCAACAACAAGCTGCAG AGG (forward primer), TGGGACTAAAAGGGTCGATG (reverse primer).

Live-Cell Imaging

For live imaging of centrosomes, worms were dissected on glass coverslips in M9 buffer and then mounted on 2% agar pads. Imaging was conducted at 25°C and carried out on a spinning-disc confocal system consisting of an Olympus IX8 inverted stand microscope body equipped with a Prior NanoScanZ, a Yokogawa CSU-X1 spinning disc head, a 488 nm solid-state laser Coherent Sapphire (50 mW), and an Andor iXon EM+ DU-897 BV back-illuminated EMCCD camera for detection. The lens used was an Olympus UPlanSApo 60×/1.20 W. The microscope was controlled by iQ 1.10.2 software.

For live imaging of cell boundaries, worms expressing a fusion between GFP and a PH domain (OD58) were dissected on glass coverslips in M9 buffer, and embryos were mounted in a capillary filled with 1% low melting point agarose in PBS with 0.1% Tween. Z stacks (x/y pixel size: 0.365 μm, z-step size: 1 μm) from three different views (0°, 120°, and 240°) were acquired at 1 min intervals using a prototype selective plane illumination microscope developed by Carl Zeiss MicroImaging and equipped with a Zeiss 40×/0.8 Achroplan objective. The individual views were fused into single views as previously described [8] to give a final pixel size of 0.365 μm in all three dimensions.

Image Analysis

For all centrosome size measurements, acquired stacks were analyzed by a custom-made algorithm [9]. To compute cell volumes from SPIM-derived images of fluorescently labeled cell membranes (PH domain::GFP), we used a marker-based 3D-watershed approach [10] for image segmentation; the volume of each segmented cell was approximated by computing its area in each image plane and modeling the volume enclosed between two adjacent planes as a prismatoid.

Growth Rates

An approximation to the time derivative at each sampling time point of the centrosome growth curves was computed by locally fitting a straight line to the curve in a window of ±60 s centered at the respective time point.

Quantitative Western Blotting

For comparing expression levels, 40 adult gravid hermaphrodites were picked into 10 μl of water and snap frozen in liquid nitrogen, then thawed, mixed with 10 μl sample buffer (125 mM Tris, [pH 6.8], 6% SDS wt/vol, 10% vol, 20% glycerol vol/vol), and loaded onto a NuPage 3%–8% Tris-Acetate gel (for SPD-2) or a NuPage Novex 4%–12% Bis-Tris gel (for AIR-1 and SPD-5) from Invitrogen. Immunoblots were probed using primary antibodies at 1 μg/ml and detected using a horseradish peroxidase (HRP)-conjugated secondary antibody (1:10,000; Bio-Rad Laboratories).

GST-Pull-Downs

All expression constructs were made using Gateway technology (Invitrogen) and Gateway-compatible baculovirus expression vectors (pDEST10 for His-tagged constructs and pDEST20 for GST-tagged constructs). Full-length PLK-1, a SPD-2 fragment (aa 103–310), and a mutated SPD-2 fragment (aa 103–310) with the substitutions S232T and T233A were expressed using the baculovirus expression system. Virus stocks for all three constructs were made according to a modified standard protocol [10] and then used to infect insect cell cultures (SF+ cells) for protein expression. After 72 hr, infected cells were harvested and lysed in extract buffer (50 mM HEPES [pH 7.4], 5% glycerol, 0.1% Triton X-100, 150 mM NaCl, protease inhibitors [Complete tablets from Roche], and phosphatase inhibitors [PhosSTOP from Roche]). Cells were crushed by pressing the cell suspension several times through a syringe. After adding Benzonase (Sigma-Aldrich) and incubation for 10 min on ice, lysates were cleared by ultracentrifugation and then incubated with Glutathione Sepharose 4 Fast Flow beads (GE LifeScience) for 2 hr at 4°C on a rotating wheel. Beads were washed three times with extract buffer and then boiled in sample buffer (125 mM Tris, [pH 6.8], 6% SDS wt/vol, 10% vol, 20% glycerol vol/vol) for 5 min at 90°C. Samples were then loaded onto NuPage Novex 4%–12% Bis-Tris gels (Invitrogen). An anti-GST antibody (GE Healthcare) and an anti-His antibody (GE Healthcare) were used for detection by western blotting. For dephosphorylation, the extract/wash buffer did not contain PhosSTOP inhibitors, and beads were incubated for 1 hr at 30°C with lambda protein phosphatase (λPP) (New England Biolabs) in extract buffer supplemented with 1 mM $MnCl_2$ prior to boiling.

Immunohistochemistry

Immunofluorescence experiments were essentially performed as described [12]. The SPD-2 antibody (MO750) was produced by immunizing two rabbits with a purified recombinant SPD-2 fragment. One hundred micrograms of the generated SPD-2 antibody was then subjected to direct labeling with Alexa 488 using the DyLight 488 Microscale Antibody Labeling Kit (Thermo Scientific). The conjugated antibody was used at a dilution of 1:50. The rabbit-derived PLK-1 antibody (gift from Andy Golden) was used at a dilution of 1:1000, and a α-rabbit secondary antibody conjugated to Alexa 594 was used at 1:1000 for visualization (Invitrogen, Molecular Probes). Samples were eventually mounted in mounting media supplemented with DAPI to stain DNA. Z stacks through embryos covering both poles and the spindle were acquired using a wide-field Delta Vision microscope (Applied Precision). Acquired stacks were analyzed by a custom-made algorithm [9] to quantify the total intensity of SPD-2 and PLK-1 at the centrosome.

Supplemental Information

Supplemental Information includes six figures, Supplemental Experimental Procedures, and two movies and can be found with this article online at doi:10.1016/j.cub.2011.06.002.

Acknowledgments

We thank Cliff Brangwynne, David Zwicker, and Frank Jülicher for essential discussions on centrosome growth. We also wish to thank Suzanne Eaton, Cliff Brangwyne, and Jordan Raff for critical reading of the manuscript; Stephan Preibisch for collaborating on SPIM imaging; and Jan Peychl and Britta Schroth-Diez for microscope support. We are also grateful to Zoltan Maliga, Mike Boxem, and Stuart Milstein for support with mapping protein-protein interactions; Horatiu Fantana for bead injections; and the Max Planck Society and the Alexander-von-Humbold Stiftung for funding.

Received: March 15, 2011
Revised: May 31, 2011
Accepted: June 1, 2011
Published online: July 28, 2011

References

1. Marshall, W.F. (2004). Cellular length control systems. Annu. Rev. Cell Dev. Biol. *20*, 677–693.
2. Hyman, A.A., and Oegema, K. (2006). Cell division. In WormBook, The *C. elegans* Research Community, ed. 10.1895/wormbook.1.72.1, http://www.wormbook.org.
3. Kemp, C.A., Kopish, K.R., Zipperlen, P., Ahringer, J., and O'Connell, K.F. (2004). Centrosome maturation and duplication in C. elegans require the coiled-coil protein SPD-2. Dev. Cell *6*, 511–523.
4. Barr, F.A., Silljé, H.H., and Nigg, E.A. (2004). Polo-like kinases and the orchestration of cell division. Nat. Rev. Mol. Cell Biol. *5*, 429–440.
5. Greenan, G., Brangwynne, C.P., Jaensch, S., Gharakhani, J., Jülicher, F., and Hyman, A.A. (2010). Centrosome size sets mitotic spindle length in Caenorhabditis elegans embryos. Curr. Biol. *20*, 353–358.
6. Mazia, D., Harris, P.J., and Bibring, T. (1960). The multiplicity of the mitotic centers and the time-course of their duplication and separation. J. Biophys. Biochem. Cytol. *7*, 1–20.
7. Sluder, G., and Rieder, C.L. (1985). Centriole number and the reproductive capacity of spindle poles. J. Cell Biol. *100*, 887–896.
8. Palazzo, R.E., Vogel, J.M., Schnackenberg, B.J., Hull, D.R., and Wu, X. (2000). Centrosome maturation. Curr. Top. Dev. Biol. *49*, 449–470.
9. Salisbury, J.L. (2003). Centrosomes: Coiled-coils organize the cell center. Curr. Biol. *13*, R88–R90.
10. Hannak, E., Kirkham, M., Hyman, A.A., and Oegema, K. (2001). Aurora-A kinase is required for centrosome maturation in Caenorhabditis elegans. J. Cell Biol. *155*, 1109–1116.
11. Pelletier, L., Özlü, N., Hannak, E., Cowan, C., Habermann, B., Ruer, M., Müller-Reichert, T., and Hyman, A.A. (2004). The Caenorhabditis elegans centrosomal protein SPD-2 is required for both pericentriolar material recruitment and centriole duplication. Curr. Biol. *14*, 863–873.
12. Hamill, D.R., Severson, A.F., Carter, J.C., and Bowerman, B. (2002). Centrosome maturation and mitotic spindle assembly in C. elegans require SPD-5, a protein with multiple coiled-coil domains. Dev. Cell *3*, 673–684.
13. Jaensch, S., Decker, M., Hyman, A.A., and Myers, E.W. (2010). Automated tracking and analysis of centrosomes in early Caenorhabditis elegans embryos. Bioinformatics *26*, i13–i20.
14. Bobinnec, Y., Fukuda, M., and Nishida, E. (2000). Identification and characterization of Caenorhabditis elegans gamma-tubulin in dividing cells and differentiated tissues. J. Cell Sci. *113*, 3747–3759.
15. Strome, S., Powers, J., Dunn, M., Reese, K., Malone, C.J., White, J., Seydoux, G., and Saxton, W. (2001). Spindle dynamics and the role of gamma-tubulin in early Caenorhabditis elegans embryos. Mol. Biol. Cell *12*, 1751–1764.
16. Hannak, E., Oegema, K., Kirkham, M., Gönczy, P., Habermann, B., and Hyman, A.A. (2002). The kinetically dominant assembly pathway for centrosomal asters in Caenorhabditis elegans is γ-tubulin dependent. J. Cell Biol. *157*, 591–602.
17. Severson, A.F., and Bowerman, B. (2003). Myosin and the PAR proteins polarize microfilament-dependent forces that shape and position mitotic spindles in Caenorhabditis elegans. J. Cell Biol. *161*, 21–26.
18. Krueger, L.E., Wu, J.C., Tsou, M.F., and Rose, L.S. (2010). LET-99 inhibits lateral posterior pulling forces during asymmetric spindle elongation in C. elegans embryos. J. Cell Biol. *189*, 481–495.
19. Schlaitz, A.L., Srayko, M., Dammermann, A., Quintin, S., Wielsch, N., MacLeod, I., de Robillard, Q., Zinke, A., Yates, J.R., 3rd, Müller-Reichert, T., et al. (2007). The C. elegans RSA complex localizes protein phosphatase 2A to centrosomes and regulates mitotic spindle assembly. Cell *128*, 115–127.
20. Hara, Y., and Kimura, A. (2009). Cell-size-dependent spindle elongation in the Caenorhabditis elegans early embryo. Curr. Biol. *19*, 1549–1554.
21. Maddox, A.S., Habermann, B., Desai, A., and Oegema, K. (2005). Distinct roles for two C. elegans anillins in the gonad and early embryo. Development *132*, 2837–2848.
22. O'Connell, K.F., Caron, C., Kopish, K.R., Hurd, D.D., Kemphues, K.J., Li, Y., and White, J.G. (2001). The C. elegans zyg-1 gene encodes a regulator of centrosome duplication with distinct maternal and paternal roles in the embryo. Cell *105*, 547–558.
23. Kirkham, M., Müller-Reichert, T., Oegema, K., Grill, S., and Hyman, A.A. (2003). SAS-4 is a C. elegans centriolar protein that controls centrosome size. Cell *112*, 575–587.
24. Pelletier, L., Müller-Reichert, T., Srayko, M., Özlü, N., Schlaitz, A., and Hyman, A.A. (2004). In Centrosomes in Development and Disease, Online Edition, E.A. Nigg, ed. (Weinheim, Germany: Wiley).
25. Zhu, F., Lawo, S., Bird, A., Pinchev, D., Ralph, A., Richter, C., Müller-Reichert, T., Kittler, R., Hyman, A.A., and Pelletier, L. (2008). The mammalian SPD-2 ortholog Cep192 regulates centrosome biogenesis. Curr. Biol. *18*, 136–141.
26. Schumacher, J.M., Ashcroft, N., Donovan, P.J., and Golden, A. (1998). A highly conserved centrosomal kinase, AIR-1, is required for accurate cell cycle progression and segregation of developmental factors in Caenorhabditis elegans embryos. Development *125*, 4391–4402.
27. Redemann, S., Schloissnig, S., Ernst, S., Pozniakowsky, A., Ayloo, S., Hyman, A.A., and Bringmann, H. (2011). Codon adaptation—based control of protein expression in C. elegans. Nat. Methods *8*, 250–252.
28. Boxem, M., Maliga, Z., Klitgord, N., Li, N., Lemmens, I., Mana, M., de Lichtervelde, L., Mul, J.D., van de Peut, D., Devos, M., et al. (2008). A protein domain-based interactome network for C. elegans early embryogenesis. Cell *134*, 534–545.
29. Ouyang, B., Wang, Y., and Wei, D. (1999). Caenorhabditis elegans contains structural homologs of human prk and plk. DNA Seq. *10*, 109–113.
30. Chase, D., Serafinas, C., Ashcroft, N., Kosinski, M., Longo, D., Ferris, D.K., and Golden, A. (2000). The polo-like kinase PLK-1 is required for nuclear envelope breakdown and the completion of meiosis in Caenorhabditis elegans. Genesis *26*, 26–41.
31. Elia, A.E.H., Cantley, L.C., and Yaffe, M.B. (2003). Proteomic screen finds pSer/pThr-binding domain localizing Plk1 to mitotic substrates. Science *299*, 1228–1231.
32. Conduit, P.T., Brunk, K., Dobbelaere, J., Dix, C.I., Lucas, E.P., and Raff, J.W. (2010). Centrioles regulate centrosome size by controlling the rate of Cnn incorporation into the PCM. Curr. Biol. *20*, 2178–2186.
33. Elia, A.E.H., Rellos, P., Haire, L.F., Chao, J.W., Ivins, F.J., Hoepker, K., Mohammad, D., Cantley, L.C., Smerdon, S.J., and Yaffe, M.B. (2003). The molecular basis for phosphodependent substrate targeting and regulation of Plks by the Polo-box domain. Cell *115*, 83–95.
34. Ubersax, J.A., Woodbury, E.L., Quang, P.N., Paraz, M., Blethrow, J.D., Shah, K., Shokat, K.M., and Morgan, D.O. (2003). Targets of the cyclin-dependent kinase Cdk1. Nature *425*, 859–864.
35. Cowan, C.R., and Hyman, A.A. (2006). Cyclin E-Cdk2 temporally regulates centrosome assembly and establishment of polarity in Caenorhabditis elegans embryos. Nat. Cell Biol. *8*, 1441–1447.
36. Lowery, D.M., Lim, D., and Yaffe, M.B. (2005). Structure and function of Polo-like kinases. Oncogene *24*, 248–259.
37. Goryachev, A.B., and Pokhilko, A.V. (2008). Dynamics of Cdc42 network embodies a Turing-type mechanism of yeast cell polarity. FEBS Lett. *582*, 1437–1443.
38. Gierer, A., and Meinhardt, H. (1972). A theory of biological pattern formation. Kybernetik *12*, 30–39.
39. Meinhardt, H., and Gierer, A. (1974). Applications of a theory of biological pattern formation based on lateral inhibition. J. Cell Sci. *15*, 321–346.
40. Boveri, T. (1905). Über die Abhängigkeit der Kerngrösse und Zellenzahl bei Seeigellarven von der Chromosomenzahl der Ausganszellen. Z. Naturw. *39*, 445–524.
41. Tanaka, K., Kanbe, T., and Kuroiwa, T. (1985). Three-dimensional behaviour of mitochondria during cell division and germ tube formation in the dimorphic yeast Candida albicans. J. Cell Sci. *73*, 207–220.
42. Dumont, S., and Mitchison, T.J. (2009). Force and length in the mitotic spindle. Curr. Biol. *19*, R749–R761.
43. Carvalho, A., Desai, A., and Oegema, K. (2009). Structural memory in the contractile ring makes the duration of cytokinesis independent of cell size. Cell *137*, 926–937.
44. Marshall, W.F., Qin, H., Rodrigo Brenni, M., and Rosenbaum, J.L. (2005). Flagellar length control system: Testing a simple model based on intraflagellar transport and turnover. Mol. Biol. Cell *16*, 270–278.
45. Stephens, R.E. (1989). Quantal tektin synthesis and ciliary length in sea-urchin embryos. J. Cell Sci. *92*, 403–413.
46. Peters, N., Perez, D.E., Song, M.H., Liu, Y., Muller-Reichert, T., Caron, C., Kemphues, K.J., and O'Connell, K.F. (2010). Control of mitotic and meiotic centriole duplication by the Plk4-related kinase ZYG-1. J. Cell Sci. *123*, 795–805.